Revista Mexicana de Astronomía y Astrofísica, **36**, 117–124 (2000)

VELOCITY STRUCTURE IN THE CURVED JET S187:SCP 1 (H2):[1]

L. Salas,[2] I. Cruz-González,[3], and M. Rosado[3]
Received 2000 January 28; accepted 2000 June 20

RESUMEN

Describimos la estructura cinemática del chorro molecular curvo S187:SCP 1 (H2). Las observaciones de la emisión de hidrógeno molecular en 2.12 μm se obtuvieron utilizando un interferómetro Fabry-Pérot con resolución espectral de 24 km s^{-1} y resolución espacial de 1.6″. La región observada de 3.6 ′ × 3.6′ contiene el jet curvo completo y otras nebulosidades H_2, como el candidato a contra jet y los objetos SCP 3 y SCP 4. Se encuentra que el jet curvo está centrado a una velocidad radial de −30 km s^{-1} y que tiene componentes cinemáticas que abarcan un intervalo de 40 km s^{-1}. Por otro lado, el candidato a contra jet y las nebulosidades SCP 3 y 4 se presentan corridos al rojo con velocidades entre −12 a 30 km s^{-1}. En este trabajo discutimos los posibles mecanismos de la curvatura del jet, ya sea producida por un viento lateral o por precesión de la fuente, a la luz de la estructura de velocidad del jet.

ABSTRACT

We describe the velocity structure of the curved outflow S187:SCP 1 (H2). Observations of the 2.12 μm molecular hydrogen emission were obtained using an IR Fabry-Pérot interferometer with a spectral resolution of 24 km s^{-1} and a spatial resolution of 1.6″. The covered region of 3.6 ′ × 3.6′ contains the entire curved-jet and several H_2 nebulosities, such as the counter-jet candidate, SCP 3 and SCP 4. The kinematics show that the curved jet is centered around a radial velocity of −30 km s^{-1} with velocity components spanning 40 km s^{-1}. On the other hand, knots SCP 3 and 4 and the counter-jet candidate appear red-shifted at velocities −12 to 30 km s^{-1}. We discuss whether the observed velocity structure favors the side-wind model or precession interpretations of the jet curvature.

Key Words: **ISM: INDIVIDUAL (S187:SCP 1 (H2):) — ISM: JETS AND OUTFLOWS — ISM: KINEMATICS AND DYNAMICS — ISM: MOLECULES — STARS: FORMATION**

1. INTRODUCTION

The curved molecular hydrogen outflow S187:SCP 1 (H2), which will be called SCP 1 for short, has been reported by Salas, Cruz-González, & Porras (1998), here on Paper I. It is shown that this extremely curved jet is an outflow visible through the emission of molecular hydrogen at 2.12 μm, in the form of 13 knots surrounded by an extended nebulosity. The outflow is well-collimated near the driving source and widens into a cone along its path. The driving source of the underlying high velocity jet is most likely a TTS (NIRS 1 in Paper I), located at the apex of the outflow. The outflow extends over a region of 76″ (0.38 pc at D = 1 kpc) and has a counter-jet candidate as reported by Noriega-Crespo & Garnavich (1997) (NG97). Paper I reported also two H_2 emission nebulosities SCP 3 and SCP 4 located east of NIRS 1. Two possible explanations to the curvature of the outflow were presented in Paper I: a precessing source or a side wind induced by a proper motion of the source. The latter was adopted due to a very good fit of the model by Cantó & Raga (1995), both to the path and to the position of the stagnation point. However, the discovery of a counter-jet candidate by NG97 questions this result, since its position is not consistent with the side wind model,

[1]Based on observations collected at the Observatorio Astronómico Nacional in San Pedro Mártir, B. C., México.

[2]Instituto de Astronomía, Universidad Nacional Autónoma de México, Ensenada, B. C., México.

[3]Instituto de Astronomía, Universidad Nacional Autónoma de México, México, D. F.

but would rather point to a precessing source.

In this paper we present the velocity structure of the molecular hydrogen outflow. On one hand, we find some evidence that the counter-jet might be indeed associated to the system, while on the other hand, we have kinematical arguments to support the identification of knot E as the stagnation point favoring the side wind model.

2. INFRARED SCANNING FABRY-PÉROT OBSERVATIONS

The molecular hydrogen scanning Fabry-Pérot observations of SCP 1 and its environment were carried out using a Queensgate Fabry-Pérot interferometer in the optical bench of the CAMILA IR spectrograph (Cruz-González et al. 1994). The details of the instrumental setup are presented in Salas et al. (1999).

The observations were obtained at the 2.1 m telescope of the Observatorio Astronómico Nacional at San Pedro Mártir, B. C., México. Images under photometric conditions were taken on January 20, 1997, with a FWHM of 1.6″. An interference filter was used to restrict the spectral range for H_2 v = 1–0 S(1) (2.122 μm, $\Delta\lambda$ = 0.02 μm). We imaged a region of $3.67' \times 3.67'$ centered on the curved jet SCP 1 that corresponds to 1.07×1.07 pc^2 at the adopted distance for S187 of 1 kpc. The optical setup allows for a scale plate of 0.86″/pix.

A set of images was obtained at 26 etalon positions that scan a single order at 9.82 km s^{-1} per channel for H_2. The observing sequence consisted of alternative imaging for each etalon position the region and the sky, located 5′ to the east. The telescope allowed that the on-source image was accurately positioned back within 1″, eliminating recentering problems. On-source and sky integration times were 60 s, sufficiently short to guarantee the cancellation of atmospheric lines at each etalon position, yet enough to acquire a good signal-to-noise. The typical 1σ noise in any image is 0.07 counts/s/pixel, while the intensity in extended emission regions of interest goes up one counts/s/pixel. The line 2.1332885 μm of the Ar lamp was observed at each etalon position for calibration, obtaining a velocity uncertainty of 1 km s^{-1} in the wavelength fit. The instrumental response was observed to be Lorentzian with a FWHM of 2.4 channels. A series of high and low illumination sky flats at each etalon position were obtained at sunset for flat fielding purposes.

3. RESULTS

The reduction procedure used to obtain velocity channel images or λ-maps of the region is described in detail in Salas et al. (1999). The spectral resolution achieved for H_2 at 2.12 μm was 24 km s^{-1}. The velocity corresponding to each channel is referred to the LSR as all velocities quoted in this paper.

Of the full set, emission from the molecular line was identified mainly in 9 channels with velocities from −66.7 km s^{-1} to 11.8 km s^{-1}. The curved jet SCP 1 is seen centered at velocity channel −27.5 km s^{-1}, with emission in channels from −47 km s^{-1} to −17.7 km s^{-1}. We can also observe the H_2 emission knots SCP 4 and SCP 3 described in Paper I to the east of the field, as well as the counter jet candidate (CJ) found by NG97 to the south of NIRS-1. All of these H_2 nebulosities or knots appear red shifted from the curved jet velocity, with velocities between −12 to 31 km s^{-1}. Figure 1 shows a composite color map of the jet region. The individual RGB colors have been obtained by adding together two channels for each color; −56.9 and −47.1 for blue, −37.3 and −27.5 for green, and −17.7 and −7.8 for red. The reason for this choice is apparent from Figure 2, where the channels that make each color are indicated at the top since it allows the best appreciation of the different velocity components in the SCP 1 jet, as we discuss further below.

Regarding the curved jet SCP 1, knots A to L are detected (see Paper I) by our Fabry-Pérot observations and are marked in Fig. 1. The only exception is knot G2, where unfortunately a star in the sky frame prevented its observations. This location is marked with an X in the figure. Knot E, which is quite extended and shows interesting velocity features, has been further divided into knots E1 (at the original position of E), E2 and E3. Knot I has also been divided into knots IN and IS. The figure also shows the other nebulosities in the field: SCP 3, SCP 4, which is extended and shows two components A and B, and the possible counter-jet (NG97) which we call CJ.

Individual spectra at the position of the knots (as given in Paper I), averaged in 3×3 pixels boxes, are presented in Fig. 2. The FWHM of the H_2 lines is typically of 4 channels (40 km s^{-1}), which is much wider than the instrumental response (2.4 channels or 23.6 km s^{-1}). The observed profiles are so wide that in order to fit the lines, three Lorentzians of the instrumental width were required. These Lorentzians are shown as dotted lines in Fig. 2. The derived intensity and velocity parameters are listed in Table 1. Intensities are given in count/s/channel/pixel and have a typical error

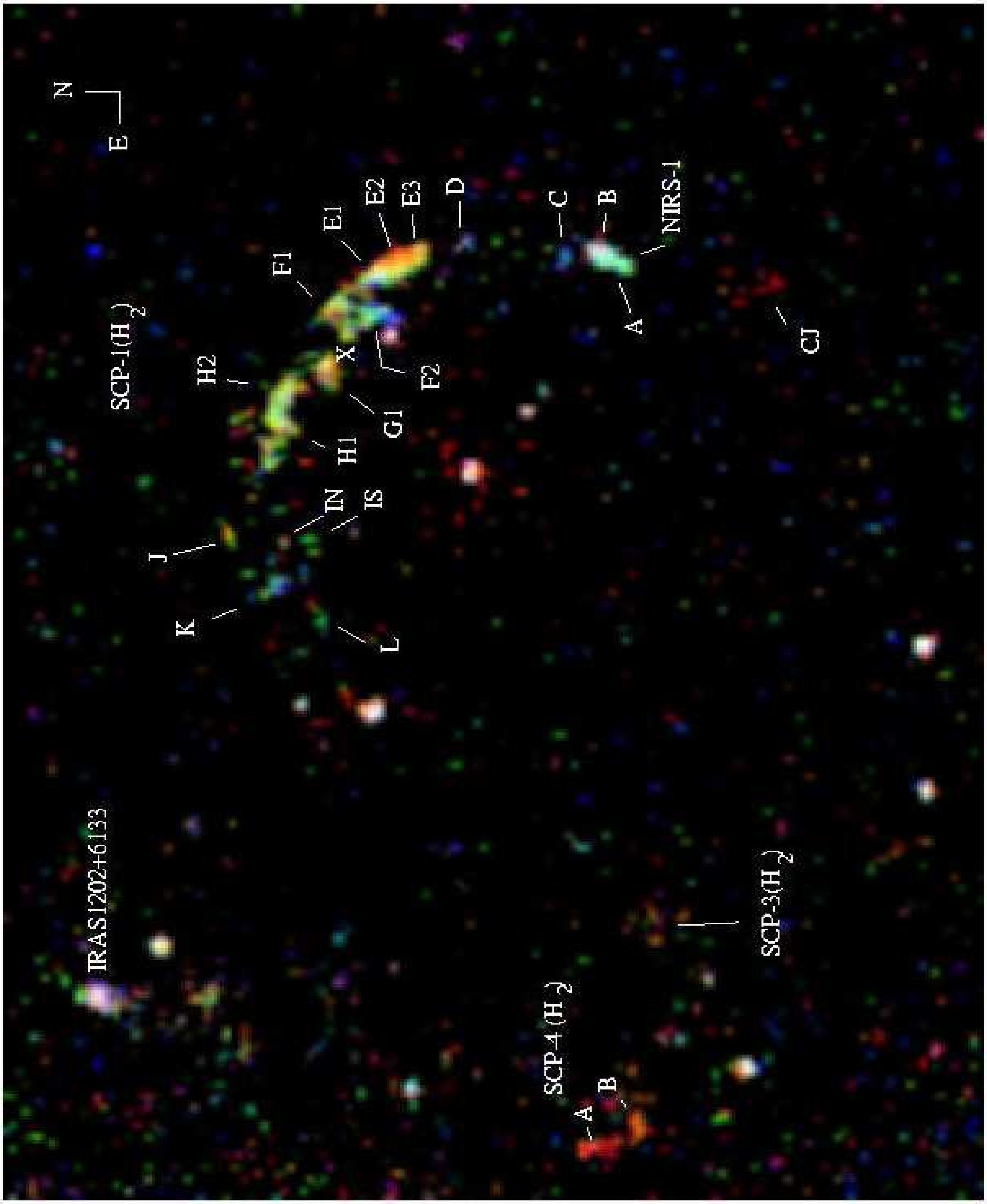

Fig. 1. Color composite of doppler shifted H_2 emission in SCP 1. Colors correspond to the velocity following ranges: Blue from -56.9 to -47.1 km s^{-1}, Green from -37.3 and -27.5 km s^{-1}, and Red from -17.7 to -7.8 km s^{-1} (LSR).

of 0.05 in these units, while velocities are given in km s^{-1} (LSR) with typical uncertainties of 5 km s^{-1}.

The LSR velocity of the molecular cloud associated to the optical H II region S187 is -14.9 km s^{-1}, according to CO measurements (Bally & Lada 1983) centered some $5'$ to the North of the jet. This velocity is indicated in Fig. 2 with a vertical dotted line. As can be seen, the components of the SCP 1 jet are blue-shifted with respect to the CO velocity, while the other nebulosities and knots are red-shifted.

If we take the CO measurements as indicative of the quiescent medium velocity, then this would indicate that CJ is most probably a counter-jet to the curved jet SCP 1 as suggested by NG97. Alternatively, since knots SCP 4 and SCP 3 have similar velocities and are aligned with CJ, they could form a separated system, farther away or more deeply embedded in the molecular cloud.

3.1. *Velocity Structure of SCP 1*

Figure 3 shows in more detail the velocity structure of knots A to F and the presence of velocity gradients in several knots. Both Fig. 2 and Fig. 3 present the complex kinematic structure observed in SCP 1 and SCP 4.

Figure 2 shows that the first knot in the chain, knot A, which coincides with the star NIRS-1, shows some continuum due to the star and one prominent velocity component at -34.6 km s^{-1} (here on, the central component). Extended blue-shifted emission is also appreciable which cannot be fitted by a single Lorentzian, steadily decreasing down to -100 km s^{-1}. Also, a red-shifted low intensity component and detached from the central component, is seen at 18.7 km s^{-1}. As one progresses to knot B the central velocity component remains but two more appear, one slightly red-shifted and another blue-shifted, with similar intensities and separated by ~ 20 km s^{-1} in each side. The red-shifted component has a velocity close to the CO velocity, which could indicate emission of material in the quiescent medium. Knots A and B are in fact connected, as can be seen in a position velocity diagram (PV) presented in Figure 4*a*. The PV diagram was constructed by introducing a 3 pixel wide "slit" centered on knot A and moving it in the direction of knot B. The contours are linearly spaced from a level 5σ above the background and in increments of 3σ. As can be seen, the red-shifted component of knot A barely makes it above the 5σ level. A clear bridge connects the central velocity component of knot A through knot B, while the red-shifted and blue-shifted components in knot B appear just there. This situation marks the presence of an obstacle in the trajectory and PV diagrams similar to this one appear in the simulations of bow shocks through the literature (see for example, Carr 1993 and Raga et al. 1995), which suggests a bow-shock structure at the position of knot B.

Knots C and D are both blue-shifted and would seem to be the continuation of the blue-shifted component in knot B. Going into knot E3, the central component reappears, but the red-shifted component becomes more important. The red-shifted component attains its maximum intensity in knot E2. E2 is at the location of the stagnation point (see Paper I), where the curvature of the jet is minimum according to the interpretation based on the side wind model. The velocity color plate (Figure 3), however, gives a more complicated picture, as velocity gradients in all directions south and east are seen. The blue-shifted velocity component appears again in knot E1, where we still have the central component and the red-shifted one starts to decrease in intensity. In Figure 4*b*, we present a position velocity diagram of knot E (from E3 to E1). This PV structure is also similar to the one of knots A-B (Fig. 4*a*), although more spatially extended and with a remarkably brighter red-shifted component. Its PV structure suggests also a bow-shock at knot E, as well as does its morphological appearance. However the modeling of this bow shock should allow for an enhanced interaction with the quiescent material at the western side of knot E2, to provide the excess red-shifted emission at this position. This enhancement would come natural in the side wind model interpretation (Paper I), since at this point the side wind is perpendicular to the jet trajectory.

It seems interesting to note that the bow-shock structure shown in the velocity color plate of knots A-B and E show a structure of high-velocity and low-velocity components which has been predicted by the models of Raga et al. (1986), where the high-velocity component precedes the low-velocity and the separation between them depends on the angle of the jet with respect to the plane of the sky.

The velocity structure is more complicated after knot E. Knot F2 is predominantly blue and the central and red-shifted components decrease in intensity and seem to mix together. This knot is also special since it is located in the internal part of the curvature. Knot F1 shows again three velocity components, but from the velocity color plate (Fig. 3), it is clear that large velocity gradients are present, and the relative importance of each component varies at different positions. The same is true for knot G1.

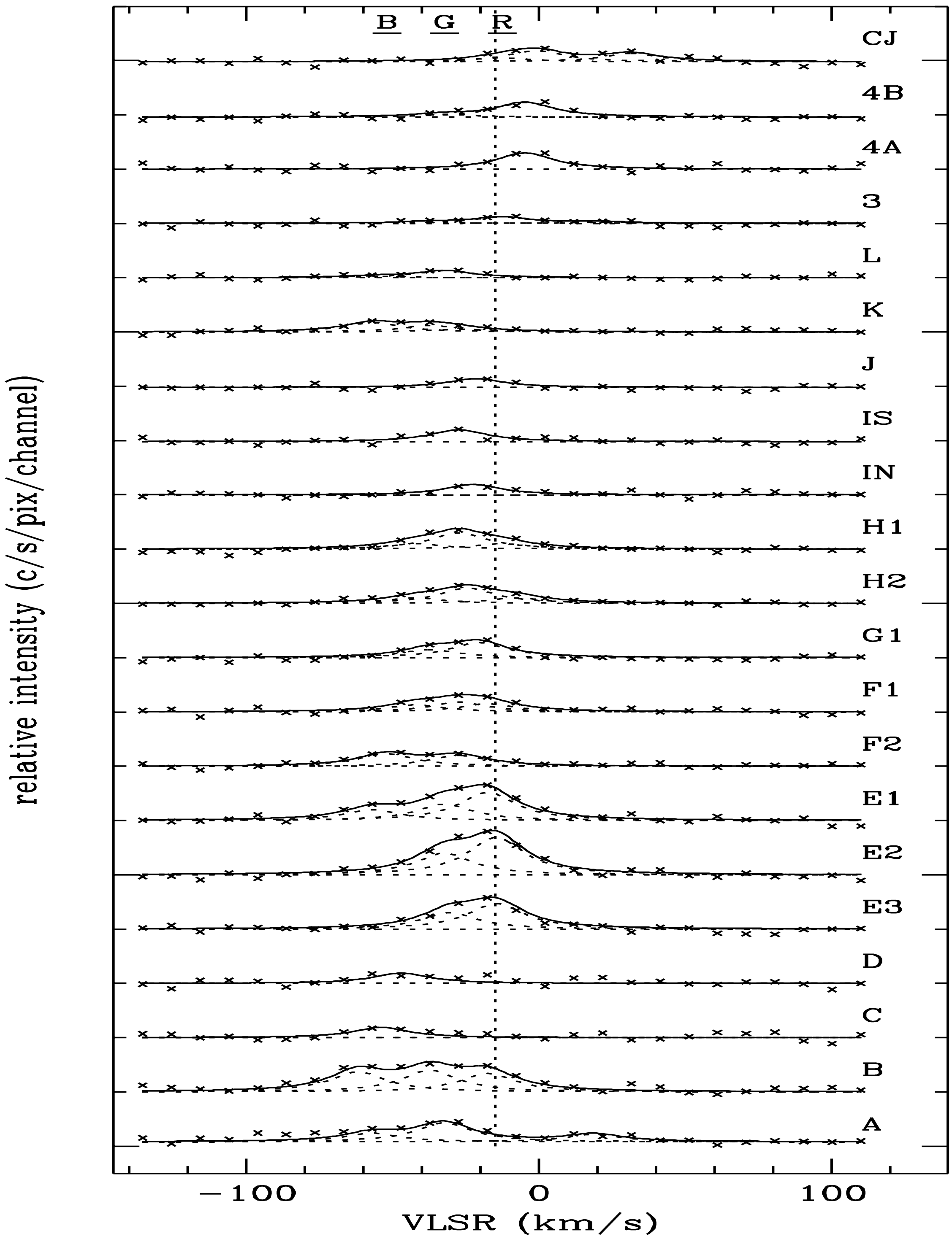

Fig. 2. Velocity components of knots A through L in SCP 1, knots SCP 3, SCP 4 (components A and B), and counter-jet candidate CJ. The vertical dotted line indicates the CO ambient velocity. Horizontal segments labeled BGR indicate the velocity ranges that make the RGB colors for Figures 1 and 3.

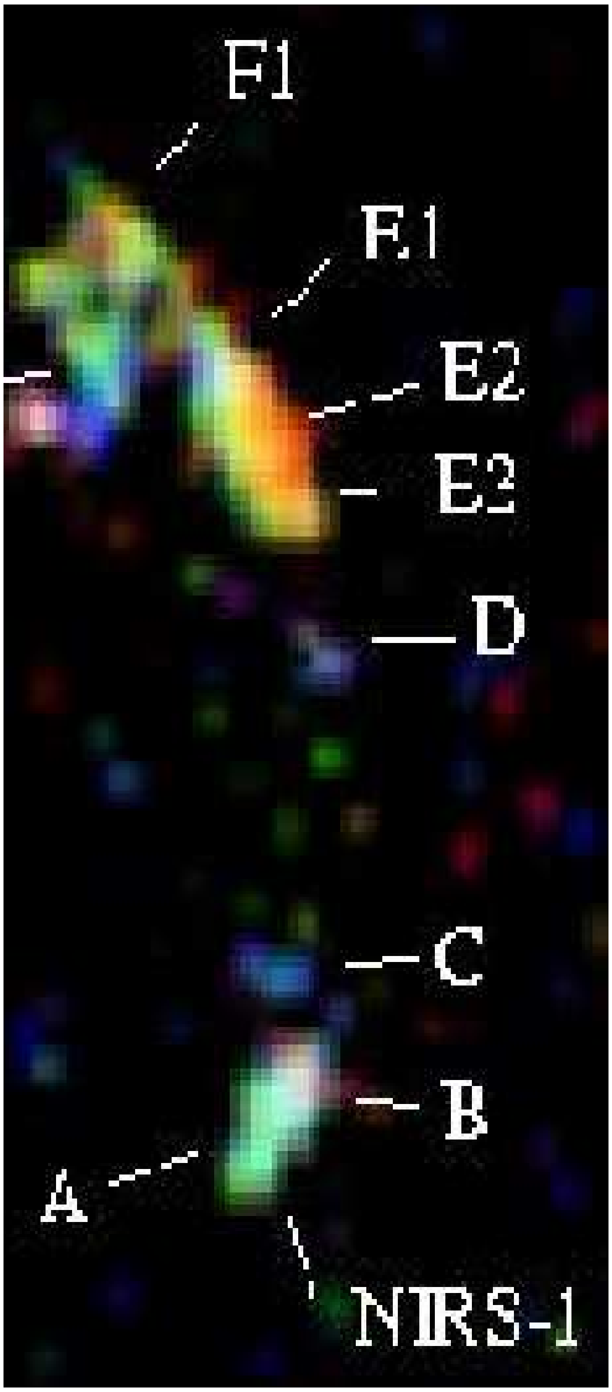

Fig. 3. Velocity color composite image of knots A to F (colors as in Figure 1).

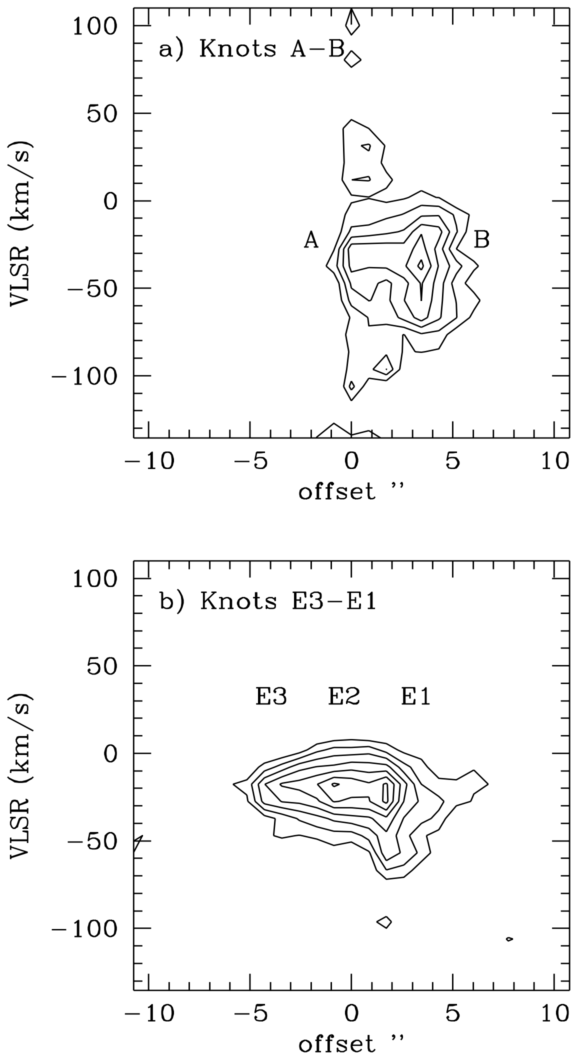

Fig. 4. Position-velocity maps of H_2 knots obtained with a 3 pixels wide "slit". On the left, *a)* Knots A to B and *b)* Knots E3 to E1. First contour is 5σ above background (σ=0.07 c/s/pix) and subsequent contours spaced in 3σ increments.

In knots H2 and H1 a central component is again seen, but this time at a velocity of ~ -25 km s^{-1}, which is 10 km s^{-1} blue-shifted to the original central component in knot A, but equally red-shifted to the CO velocity. In knots I, J, K, and L the central component wiggles around -21 to -37 km s^{-1}, although blue-shifted components are visible in knots K and L.

3.2. *Velocity Structure of SCP 3, SCP 4, and CJ Candidate*

For objects SCP 3 and SCP 4, the main component is red-shifted with respect to the CO velocity (at −13 and −5 km s^{-1}), but they also have a weak component close to the central velocity component in knot A.

The counter-jet candidate velocities are even redder, with two main components at velocities −0.9 and 31.4 km s^{-1}, which are equally separated from the weak red-shifted component in knot A (at 18.6 km s^{-1}). The presence of this red-shifted component in knot A and CJ could be an indication that the counter-jet is being produced by the star NIRS-1 as well and a possible relation between knot A and CJ. The CJ shows also a blue-shifted component with velocity close to the CO velocity, again possibly indicating emission from material in the quiescent medium.

4. DISCUSSION

Many uncertainties remain that hamper an integral view of the region. For example, if the red-shifted component in knot A would be real it could indicate a kinematic connection with the counter-jet candidate. In this case, we would also have to accept that the two velocity components of CJ, none of which coincides with those of knot A, are related to it. Furthermore, if the CJ is indeed a counter-jet then the curvature of the outflow should be due to a rather large precession movement of the source. If this is so, there would be no explanation for the enhancement of the red-shifted component in knot E. Alternatively, if we accept the side wind model of Cantó & Raga (1995) for the curvature of the outflow, the enhancement of the red-shifted component in knot E coincides with the position of the stagnation point along the trajectory as derived from this model (see Paper I). However, in this case it would be impossible to reconcile the position of CJ if it were a true counter-jet. A different origin of CJ would thus be needed, an a possibility is that it shares a common origin with objects SCP 3 and SCP 4, since CJ is aligned with them and has similar velocities, all red-shifted to the quiescent CO velocity.

Whatever the source of the curvature, we observe that the velocity structure of the curved outflow is characterized by a wide spread in velocity, consistent with three components separated by $\sim$ 20 km s^{-1} each. A central component at the source seems to prevail along the jet, while the red-shifted one is close to the CO velocity and would indicate emission of material in the quiescent medium. The velocity structure found for several knots along the jet support a common origin and a kinematic association.

TABLE 1

THREE VELOCITY COMPONENTS OF H_2 KNOTS IN S187

Knot[a]	v_3[b]	I_3[c]	v_2[b]	I_2[c]	v_1[b]	I_1[c]
1(H2):A	−57.0[d]	0.16	−32.4	0.35	18.7	0.14
1(H2):B	−61.9	0.37	−37.3	0.4	−17.7	0.34
1(H2):C	−54.0	0.19	⋯	⋯	⋯	⋯
1(H2):D	−47.1	0.19	⋯	⋯	⋯	⋯
1(H2):E3[e]	⋯	⋯	−30.4	0.3	−14.7	0.47
1(H2):E2[e]	⋯	⋯	−32.4	0.4	−14.7	0.69
1(H2):E1[e]	−56.9	0.2	−32.4	0.3	−17.7	0.52
1(H2):F2	−52.0	0.23	−27.5	0.2	⋯	⋯
1(H2):F1	−42.2	0.13	−27.5	0.18	−17.7	0.15
1(H2):G1	−37.3	0.15	−20.6	0.28	⋯	⋯
1(H2):H2	−42.2	0.1	−24.5	0.28	−7.8	0.1
1(H2):H1	−42.2	0.1	−27.5	0.3	−12.8	0.1
1(H2):IN	⋯	⋯	−22.6	0.19	⋯	⋯
1(H2):IS	⋯	⋯	−27.5	0.22	⋯	⋯
1(H2):J	⋯	⋯	−21.6	0.16	⋯	⋯
1(H2):K	−56.9	0.17	−37.3	0.12	−27.5	0.05
1(H2):L	−56.9	0.03	−32.4	0.13	⋯	⋯
3(H2)	−37.3	0.03	−12.7	0.12	21.6	0.03
4(H2):A	⋯	⋯	−4.9	0.3	⋯	⋯
4(H2):B	−32.4	0.05	−4.9	0.27	⋯	⋯
CJ[f]	−12.8	0.07	−1.0	0.2	31.4	0.15

[a]Knots in H_2 nebulosities, clarify source designation in Salas, Cruz-González, & Porras 1998.
[b]LSR velocities in km s^{-1}.
[c]Intensities in counts/sec/channel/pixel, averaged in boxes of 3×3 pixels.
[d]This component is not well fitted, it has extended blue emission.
[e]Part of extended component E, subdivided into kots E1, E2, and E3.
[f]Counter-jet candidate, Noriega-Crespo & Garnavich 1997.

Knots A-B and E show kinematic evidence of bow-shock structure, since its PV diagrams are similar to other cases in the literature. The H_2 emission in HH 7 has been modeled by Carr (1993) as a J-type bow-shock with a magnetic precursor. In this model, low-velocity emission comes from material accelerated by the magnetic precursor from quiescence to a fraction of the oblique shock velocity, while some high-velocity emission arises at the post-shock cooling region, either by reformation or survival to the J-shock. The theoretical PV diagram for HH 7 is quite similar to the PV diagrams of knots A-B and

E in SCP 1. However, recent ISO observations of HH 7–11 outflow (Molinari et al. 2000), suggest that a mix of J and C shocks prevail in HH 7, and the pure rotational hydrogen lines should be produced instead by C shocks in the wings of the bow shock. The simulations presented by Raga et al. (1995) for the heads of HH jets, assuming J-type shocks and no magnetic fields, provide PV diagrams for H_2 that resemble also the observed ones in SCP 1. In this case, molecular hydrogen is destroyed at the tip of the bow shock and emission comes mainly from the wings of the bow. A good fit to the observed PV diagram would also be expected from a C shock, where depending on the magnetic field strength and orientation, H_2 might be able to survive the shock at the tip of the bow, and even if not, it would be excited at the wings, thus producing similar PV diagrams to those of Carr (1993) or Raga et al. (1995). The question of whether J or C shocks are responsible for the H_2 emission in SCP 1 clearly cannot be answered here. The observation of other molecular, atomic and ionic lines in the curved jet SCP 1 is needed.

5. CONCLUSIONS

We have presented the velocity structure of the 2.12 μm H_2 line for the curved molecular outflow S187:SCP 1 (H2). The possible connection with the counter-jet candidate of NG97 has been discussed in the light of a possible kinematical connection. The confirmation of this connection would hamper the side-wind model interpretation for the curvature of the jet, and would in turn, favor a precessing source as the cause of such extreme curvature. However, the velocity structure of knot E, the stagnation point of the side-wind curved jet, supports the lateral wind interaction. Thus, the situation remains unclear and further studies will be required to elucidate this question. The velocity structure found for several knots along the jet support a common origin and a kinematic association.

Along the curved jet, bow-shocks are identified at the position of knots A-B and E, since they show a characteristic position-velocity structure, as well as some morphological evidence. Reasonable fits to bow-shock structure are found in the literature, but it is at present impossible to decide for any, since the question of whether J or C shocks prevail, remains unanswered. The curved molecular outflow S187:SCP 1 (H2) is an excellent candidate for detail modeling and the observation of other molecular, atomic and ionic lines.

Our thanks to R. Costero for his work and effort in the acquisition of the etalon. We acknowledge the support work of the OAN/SPM technical group and night assistants F. Montalvo and G. García. This research has been financed by grant IN–120198 from DGAPA (UNAM). The referee comments are greatly appreciated.

REFERENCES

Bally, J., & Lada, C. J. 1983, ApJ, 265, 824
Cantó, J., & Raga, A. C. 1995, MNRAS, 277, 1120
Carr, J. S. 1993, ApJ, 406, 553
Cruz-González, I., et al. 1994, in Instrumentation in Astronomy VIII, (CAMILA: Infrared Camera/Spectrograph for OAN-SPM), eds. D. L. Crawford & E. R. Craine, Proc. SPIE 2198, p. 774
Molinari, S., Noriega-Crespo, A., Ceccarelli, C., Nisini, B., Giannini, T., Lorensetti, D., Caux, E., Liseau, R., Saraceno, P., & White, G. J. 2000, ApJ, in press (astro-ph/003031)
Noriega-Crespo, A., & Garnavich, P. M. 1997, BAAS, 191, #129.09 (NG97)
Raga, A. C., Böhm, K. H., Solf, J. 1986, AJ, 92, 119
Raga, A., Taylor, S. D., Cabrit, S., & Biro, S. 1995, A&A, 296, 833
Salas, L., Cruz-González, I, & Porras, A. 1998, ApJ, 500, 853 (Paper I)
Salas, L., Rosado, M., Cruz-González, I., Gutiérrez, L., Valdez, J., Bernal, A., Luna, E., Ruiz, E., & Lazo, F. 1999, ApJ, 511, 822

Irene Cruz-González and Margarita Rosado: Instituto de Astronomía, UNAM, Apartado. Postal 70-264, 04510 México, D. F. 04510, México (irene,margarita@astroscu.unam.mx).
Luis Salas: Instituto de Astronomía, Observatorio Astronómico Nacional, UNAM, Apartado Postal 877, 22830 Ensenada, B. C., México (salas@astrosen.unam.mx).